Composite Structures 207 (2019) 72–80

Contents lists available at ScienceDirect

Composite Structures

journal homepage: www.elsevier.com/locate/compstruct

Matrix-graded and fibre-steered composites to tackle stress concentrations

David Stanier[a], Arjun Radhakrishnan[a], Ian Gent[a], Sree Shankhachur Roy[b], Ian Hamerton[a], Prasad Potluri[b], Fabrizio Scarpa[a], Milo Shaffer[c], Dmitry S. Ivanov[a,*]

[a] Bristol Composites Institute (ACCIS), University of Bristol, Queen's Building, University Walk, Bristol BS8 1TR, UK
[b] Robotics & Textile Composites Group, School of Materials, The University of Manchester, James Lighthill Building-E1D, Manchester M13 9PL, UK
[c] Department of Chemistry, Imperial College London, Kensington, London SW7 2AZ, UK

ARTICLE INFO

Keywords:
Graded materials
Liquid Resin Printing
Damage tolerance
Multi-matrix composites

ABSTRACT

This paper studies the feasibility of improving structural performance of composites in the presence of stress concentrators. ***Matrix grading*** through local deposition of additive-enhanced matrices and ***fibre steering*** by varying fibrous architecture are examined independently and in combination on a glass-fibre triaxial braided composite subjected to open hole tensile test. Stiffened and toughened matrices were incorporated through precise point-wise injections of liquid reactive resin into dry preforms (Liquid Resin Printing). Fibre steering was implemented by varying the braiding angle along the length of the braided sleeve. It has been shown that these novel forms of architecture modification enable a significant improvement in composite strength through a variety of deformation mechanisms. This includes local stiffening of composite in the direct vicinity of the stress concentrator and damage accumulation away from the stress concentrators. The experimental observations are explained by using simple finite-element models.

1. Introduction

Grading material properties is known to enhance mechanical performance of components with stress concentration features. The concept is widely adapted when joining dissimilar materials, *e.g.* in functional multi-material coatings, interphases and adhesive joints [1,2]. The advantages of grading are also documented for ceramics [3], polymers [4], and natural materials [5]. The primary purpose of grading is to attenuate the contrast in stiffness between joined materials; suppress stress concentration at edges, notches, or cuts; decrease residual/thermal stresses. As a result, it can improve toughness, hardness, strength, and damage resilience. An interesting example of achieving synergetic effects by applying grading in adhesive joints was shown by Carbas et al. [2]. The strength of the bond with varying glass transition temperatures (and related stiffness) was reported to exceed the properties achieved by using uniformly cured samples with either high or low glass transition temperatures.

In contrast to other materials, grading of composites with continuous reinforcement has not been extensively discussed. Partially this apparent gap is related to the terminology; if grading is interpreted as any local modification of composite properties, then many forms of fibre steering could be classified as grading (*e.g.* through automatic fibre deposition or varying the internal architecture of textile preforms through the component length [6]). On the other hand, grading of composites matrices had not been considered because of the absence of manufacturing methods for its implementation. The methods suitable for conventional engineering materials, such as powder stacking, laser sintering, slurry dipping and 3D printing [7], cannot be readily adapted to conventional composite manufacturing.

To improve the structural performance of materials in the presence of stress concentrators, grading both through steering and through matrix modification may be of interest. Steering of continuous reinforcements provides a strong variation of the material properties which is beneficial for load flow optimisation. However, it can only be implemented at a relatively large scale: the characteristic steering radius of conventional automatic fibre placement machines is in the tens of centimetres/metres. Other fibre placement techniques, such as tow steering, can be more local, but smaller radius may result in wrinkles, resin rich zones, thickness variation, and other defects. Grading of matrices, on the other hand, can potentially be much more local and suitable to suppress sharp stress gradients, which are of millimetre scale around typical bolted joints. However, grading requires to achieve a pronounced variation in local composite stiffness, which is more difficult to implement by varying the properties of matrix.

* Corresponding author.
E-mail address: dmitry.ivanov@bristol.ac.uk (D.S. Ivanov).
URL: http://www.bristol.ac.uk/composites/ (D.S. Ivanov).

https://doi.org/10.1016/j.compstruct.2018.09.019
Received 9 April 2018; Received in revised form 29 August 2018; Accepted 17 September 2018
Available online 18 September 2018

Matrix grading requires different systems to be combined in one component; only a few processing techniques are suitable. The relevant examples include co-injection Resin Transfer Moulding (RTM) [8–10], where the plies are separated by an impermeable layer, or the recently suggested Hybrid-Matrix-RTM [11], where dissimilar matrices are co-infused and separated by applying additional tooling pressure on the boundary between the two domains. Another concept, which will be considered in this study, is Liquid Resin Printing (LRP) [12,13]. In this approach, resin is injected at a predefined depth through a surgical needle. The sequential printing of the resin through the thickness allows the material to be infused locally, whilst the location of the patches in-plane can be programmed directly. This approach enables the creation of patterned, multi-matrix composite systems with internal fibre-bridged interfaces.

The ability to integrate the resins selectively allows the matrix properties to be modified at critical regions. Injected resins can be enhanced with structural micro- and nano additives. Compared to conventional processes, higher loadings of additives in the injected resin can be implemented despite their higher viscosity due to the shorter flow lengths. As a result, higher contrast in graded properties can potentially be achieved. It is expected that the non-uniformly distributed micro- or nano-scale additives will affect stiffness and stress concentration in the matrix at the micro-scale. In addition, this technique of combining matrices offers new opportunities for manipulating damage accumulation mechanisms. As shown previously, these fibre-bridged interfaces can both trigger delamination and arrest it [12]. The grading of matrices in LRP can be achieved by different methods. The trials presented in this paper relied on the natural mechanisms of grading through particle filtering around the injection site, occurring during unconstrained capillary flow. The zone on the patch boundary, where infused and injected matrix shares space, creates an additional transition in stiffness.

Open hole tests were used to assess the potential of grading composite matrices. The relation between damage accumulation mechanisms and composite strength can be rather complicated and the implications of stiffening or toughening in the vicinity of a stress concentrator are not trivial. Wisnom and Hallett [14], provided important insights on these phenomena for conventional unidirectional prepreg-based laminates subjected to open hole tests. They demonstrated that more extensive damage in the vicinity of a feature, such as delaminations, can sometimes have a strong positive effect on composite strength due to reducing stress concentration in the vicinity of the hole.

The introduction of different matrix systems in the patch can potentially lead to various consequences. For instance, a stiffer matrix may carry a larger fraction of the load, trigger earlier splitting and damage (with positive or negative implications) and redistribute the stress away from the stress concentrator effectively. On the other hand, a tougher matrix may reduce the stress concentration and suppress or delay delamination propagation, but cause premature fibre fracture. This study was set to examine which scenarios may prevail. Several systems with distinctly different properties were used to assess the impact of patch properties on the damage accumulation mechanisms, including relatively soft rubber particles and rigid nano-fibres.

In addition to matrix grading, this paper considers the possibility of enhancing the local properties through fibre steering. The steering was implemented as part of the braiding process, where the braiding angle was varied along the length of the sample from a quasi-isotropic configuration at the grips, to a more damage resilient fibre arrangement near the hole. The two instruments for stiffness distribution are then tested in conjunction and shown to achieve a remarkable synergy during damage accumulation.

This paper builds on a previous preliminary study [15], but extends the range of systems compared and develops the analysis of these architectures. It presents manufacturing trials, explores the peculiarity of the matrix-graded and fibre-steered architectures, and provides insight into the deformation mechanisms occurring in the graded composites. Simple finite element models are then used to explain the observed effects. Finally, we assess the feasibility of creating a more resilient material by altering properties in structurally critical locations.

2. Manufacturing of continuous fibre matrix-graded materials

The manufacturing trials described below are aimed at integrating various resin systems into textile baseline and steered preforms. The LRP process was first used to print resin patches into a dry textile preform, followed by consolidation, curing and then a conventional vacuum assisted resin infusion process. Resins for the patches were selected to generate a high contrast in properties with the host or infused resin on the one hand, while being processable (which sets constraints on viscosity, dispersion quality, and pot life) on the other. The volume of the injection was selected to control the size of the patches, which had to exceed the size of the holes but be smaller than the sample width. The textile preforms were selected based on considerations of density, coverage and symmetry.

2.1. Liquid Resin Print (LRP) process

The concept of liquid resin print can be briefly summarised as follows. Resin is injected through a steel needle (21 G, 0.5 mm inner diameter) at a predefined depth using a recently developed printing concept [12,13]. Each injection impregnates a thin layer of the preform around the injection site. A series of these injections through the preform thickness creates an impregnated area which, upon pressure and heat assisted consolidation, cures into a solid patch. In a subsequent liquid moulding process, the fibre-bridged interfaces between the injected and infused resins are formed. Any reactive resin can be injected if it maintains sufficiently low viscosity at the time scales and temperatures of injection. The injected resins can also be functionalized, reinforced and toughened with dispersed micro- or nanoparticles providing that the viscosity of the injected solution is still reasonably low, and the particle or cluster size does not exceed the needle diameter.

The print process allows a wide range of parameters and internal properties to be investigated, enabling the material designer to apply tough, ductile or stiff systems around a feature. The size of the patch is controlled by the injected volume of resin and the patch morphology is determined by the consolidation programme. The interface between the patch and host matrix can also be manipulated. Hence, the transition in properties can be abrupt or smooth depending on the preform architecture, the constraints of the preform during the injection procedure, thermal treatment of the injected resin and consolidation parameters. In the current study, the patch infusion during printing relied on unconstrained capillary flow and natural filtration mechanisms in the uncompacted preform. At least three injections through the ply thickness were delivered in order to ensure a continuously impregnated patch.

2.2. Matrix systems selected for patching

Three thermosetting solutions were explored for the patches: a homogenous high glass transition temperature (T_g) cyanate ester resin, a low T_g resin system toughened with rubber particles, and an epoxy resin stiffened with carbon nanotubes (CNT). These resin systems cover a wider range of material properties in terms of stiffness, thermal stresses at the microlevel, and ductility. At this stage, it was important to assess which of these properties may appear critical for overall performance and exhibit greater potential through steering damage accumulation mechanisms, improving strength or strain to failure. The printing program comprised 10 injections of 12.5 µl each, with each injection spaced at 0.5 mm above the previous one. The material systems were:

a) 1,1-*bis*(4-Cyanatophenyl)ethane cyanate ester (CE), is a commercial system (Primset™ LECY, Lonza, Visp, Switzerland) with a high T_g of 289 °C and mechanical properties similar to the epoxy (tensile modulus: 3.2 GPa, tensile strength: 88 MPa, strain to failure: 3.2% [16], flexural strain to failure 4.3% [17]). Owing to its higher T_g, the system, as a composite matrix, is likely to exhibit a higher level of thermal stress compared to the host matrix. After injection, the resin was cured under a press according to the recommended schedule: one hour at 150 °C, then ramped to 200 °C and dwelled at this temperature for three hours, finally post-cured at 260 °C for an hour in the oven. The patches produced with this resin will be referred to as 'CE patch'.
b) PRIME™ 20LV (Gurit) toughened with cross-linked core-shell silicone particles GENIOPERL® P52 (Wacker), which constitutes an organic acrylic shell enveloping a siloxane core. The particles are dispersed using a shear mixer (T10-IKA) operating at 30,000 rpm to reach a loading of 6 wt%. The average agglomerate size of the powder is 30–100 μm, with a primary particle size of approximately 200 nm according to the data sheet. The system was degassed prior to mixing with the hardener. The patches were printed and then cured using the recommended schedule at 70 °C for 6 h. The patches produced with this system will henceforth be referred to as 'CSP patch'.
c) CNT-rich powder developed by Herceg et al. [18] through cryo-milling of a highly loaded, yet well dispersed CNT suspension of 15% wt. The advantage of using powder is that a suspension of equivalent CNT loading has lower viscosity than a uniformly homogenised liquid system due to lower aspect ratio of the particles. The suspension is based on a solid DGEBA based epoxy resin, Araldite R GT7071 (Huntsman), with a dicyandiamide (DICY) based solid curing agent Dyhard R 100S and multi-wall carbon nanotubes NC7000TM (Nanocyl). The CNTs are blended using a twin-screw extruder and followed by cryo jet milling of the extruded mixture. A filter was used to screen the particle size and aim at a characteristic size of ~20 μm [19]. The injected solution was prepared using 10 wt % of powder suspended in a second, carrier epoxy system, resulting in a final CNT content of 1.5 wt%. The carrier consisted of Araldite LY 1564 (Huntsman) mixed with 10 wt% of monoepoxide diluent, glycidyl-2-methylphenyl ether (Sigma Aldrich) and crosslinking agent Aradur 22962 (Huntsman). The system was degassed for less than 30 min and then injected into the textile preform. Upon printing and consolidation, the patches were cured for 15 min at 120 °C and then for 2 h at 150 °C. The resin system has an ultimate T_g of 116 °C. The patches produced with this system will henceforth be referred to as 'CNT Patch'.

The creation of patches was followed by conventional liquid resin infusion with flexible tooling. Low viscosity, Prime™ 20LV with extra slow hardener (manufactured by Gurit) was selected as a host matrix. The resin has a low glass transition temperature (83 °C) and good mechanical properties (stiffness 3.5 GPa, tensile strength 73 MPa, and strain to failure 3.5%). The infused resin was cured at 70 °C for 6 h. Morphology and description of patch features with comparable manufacturing procedures were reported previously [12,13]. A low level of micro-porosity is typical for printed patches due to unsaturated capillarity-driven flow during injections. The 6-mm hole was drilled through the centre of the patch of the fully infused samples as shown in Fig. 1.

2.3. Braided preforms

A triaxially braided, glass preform, manufactured at the University of Manchester was used as the reinforcement. The preforms were braided in a regular pattern with a braiding angle of ± 60° (± 0.5° is the variation of the braiding angle), 20% weight fraction of axial yarns, and 97–99% coverage of the surface (*i.e.* no significant inter-yarn fibre free space within the ply). The measured areal density of the preform was 618 g/m^2 with 600 tex, both for braiding and axial yarns (roving type Hybon 2001). The braiding yarn width was approximately 1.9 mm, the width of the axial yarn constituted 2.2 mm, and the spacing between axial yarns was 4.9 mm.

In addition to the baseline preform, a fibre steered braided preform was manufactured. Steering from 0/ ± 60° to 0/ ± 45° does not significantly affect the stress concentration factor at the macro scale. However, the braiding angle affects the damage mechanisms at early stages of deformation. A more intensive intra-yarn crack density accumulation can be expected for 60° yarns while crack density in 45° yarns is known to be limited [20] and likely to be superseded by matrix plasticity. Hence, implementation of steering was particularly interesting from the viewpoint of material performance at the advanced deformation stages.

This steering was implemented through varying the speed of braiding. In the steered (angle graded) configuration, the braiding angle was varied from ± 60° (at both ends of the sample) to ± 45° (towards the centre of the sample). The angle of ± 45° was set constant over a span of approximately 100 mm, with a transition area length of about 30–60 mm on each side as shown in Fig. 2. The areal density of the ± 45° zone was about 525 g/m^2, with 95% surface coverage. Four ply laminates were constructed for both the steered and non-steered configurations, which produced composites of nominal thickness 2.2 mm for the reference configuration and 1.8 mm in the location of ± 45° steering.

3. Mechanical testing

In a quasi-isotropic laminate, the open hole test creates a stress concentration which is roughly 3 times higher than the stress away from the hole and fades at a distance comparable to the hole size. This dictates the acceptable hole size to specimen width ratio. The sample dimensions for the open hole were defined using the guidelines of ASTM D5766/D5766M-11 standard, thereby taking a specimen width of 36 mm, and a hole size of 6 mm. The gauge length was selected to be 100 mm for the reference configuration, and 200 mm for the steered configurations, to accommodate the variation in braiding angle. Glass-epoxy woven end tabs of 2 mm thickness and 50 mm span length were used.

Half of each sample (from the centre of the hole downwards) was speckled black over a white background to ease strain recognition. The other half of the samples was used for *in-situ* observation of crack accumulation in the transmitted light image. 3D Digital Image Correlation (DIC) measurements were conducted using a commercially available Dantec Q400 system equipped with 5-megapixel cameras. The top side of the samples were used to observe damage growth through the transmitted light. The displacement was calculated using a subset size of 0.5 mm.

At least four samples of each configuration were tested. The sample strength was calculated by normalising the loads at failure with respect to the cross-sectional area of the sample in the narrowest location (*i.e.* 30 mm width). The macro strain was calculated by averaging the longitudinal strain field over the entire area of observation. To reduce the noise of measurements and build the stress-strain diagrams, the strain histories were fitted with a 4th order polynomial, and fitted to the stress-time curve using the obtained analytical dependencies (the lowest coefficient of determination among all the samples was 0.99). The apparent stiffness of the samples was then calculated using a linear regression fitted in the 0.1–0.3% macro strain range. The stress-strain curves in the range of 0 to 0.1% strain may be subjected to a higher error due to the precision of the polynomial fit, and should be treated with caution.

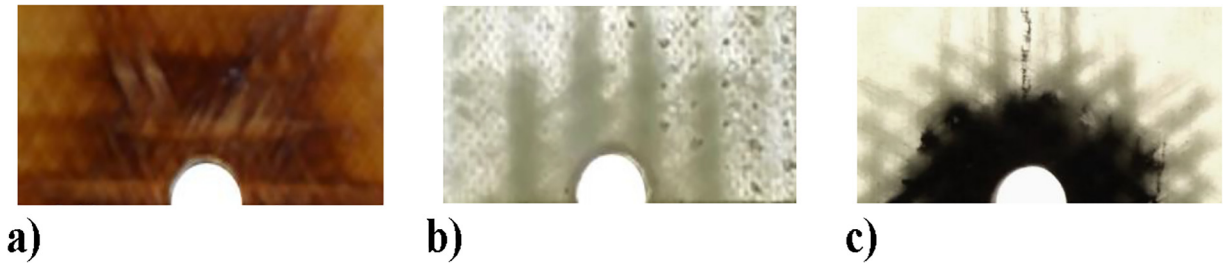

Fig. 1. Patches of various configuration in the open hole samples (half patch is shown, the hole diameter is 6 mm) a) CE patch (infused resin changed its colour because of the interaction with the patch), b) CSP Patch, c) CNT patch.

3.1. The effect of matric grading on non-steered samples

The stress-strain curves observed for these materials are notably non-linear, which is typical for textile glass-epoxy composites. Non-linearity is associated with the intra-yarn matrix cracking occurring at relatively small levels of strain. The first significant change of the slope in the referenced samples can be observed at around 0.5% strain and is caused by damage in the braiding yarns – Fig. 3a. A similar trend of the stress-strain curves was observed for CE-patched samples – Fig. 3a, though the tangent stiffness in CE samples appears to be higher after cracking started. Damage in the other patched composites started earlier: at 0.3% strain for CSP patch and at around 0.1% for the CNT patches – Fig. 3b and c. Hence, even though the instant stiffness up to 0.1–0.2% strain was systematically higher for the CNT patched samples, the apparent tangent stiffness calculated within 0.1–0.3% strain is consistently lower compared to the reference samples – Table 1.

Cracking in braiding yarns was the dominant failure mode, with localised delamination occurring not long before fibre fracture. In the reference samples, crack density was accumulated in four symmetrical bands spreading from the hole at angles of 25–70° to the direction of loading – Fig. 4. The segments from −25° to +25° in close proximity to the hole remained almost free of cracking until fibre rupture. Obviously, the crack-free segment occurred due to the traction free surface on the upper and lower sides of the hole. On the other hand, no clear crack pattern could be observed in the patched samples. Outside the patches, the crack distribution was relatively homogeneous as observed in the transmitted light images.

At the point of fibre rupture, the CSP patch samples showed an average 17% increase in strength compared to the reference samples, and a 24% increase for the CNT patched composite samples – Fig. 3, Table 1. A significant difference was found for the samples enhanced through CNT patching. The improvement in strength correlated with a consistent increase in strain to failure, and was particularly pronounced for the CNT patches.

It was observed that the hole size in the deformed reference and patched samples differed. The aspect ratio of the hole at the same level of deformation was about 5–10% larger in the reference samples than in the patched samples indicating a much higher level of local deformation – Table 2, Fig. 5. A consistently greater local deformation was observed throughout the entire deformation process.

3.2. The effect of matric grading on steered samples

The steered samples were tested in three configurations: with no patch, CSP, and CNT patch produced by the same printing procedure as for the non-steered configuration. The samples without patches showed an apparent improvement in strength – Table 3, Fig. 6. However, this effect was only due to the smaller thickness, and hence cross-sectional area, of the 0°/ ± 45° braid compared to 0°/ ± 60° (1.8 mm *vs.* 2.2 mm). The load at failure for fibre steered and non-steered configuration was approximately the same for the compared matrix/patch system.

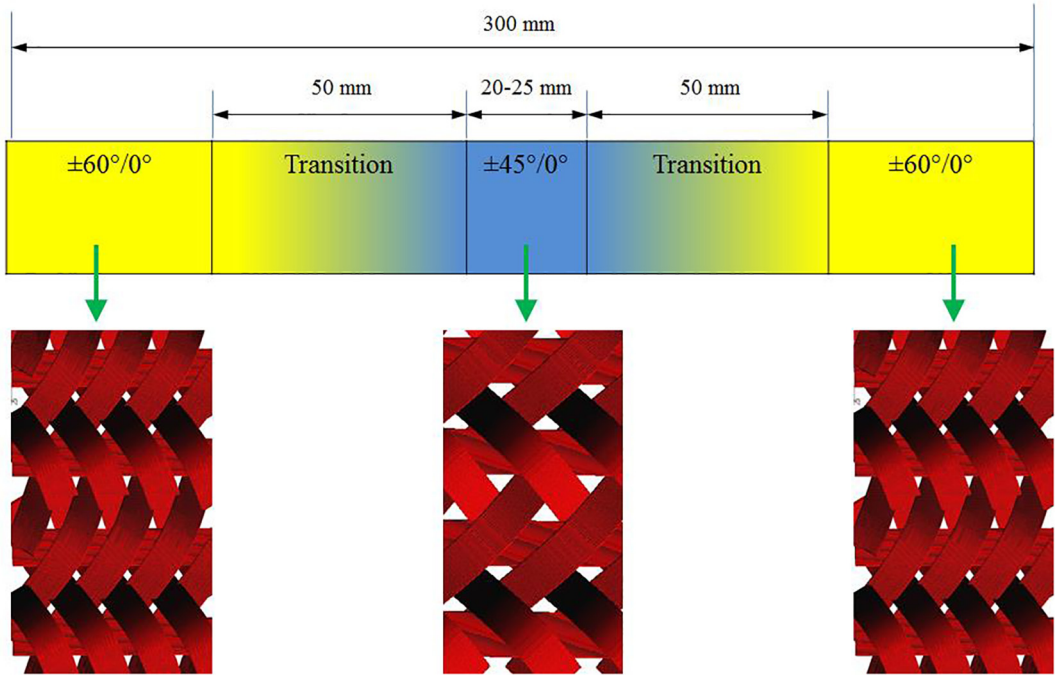

Fig. 2. A scheme of a steered (fibre-graded) sleeve produced by varying the braiding speed.

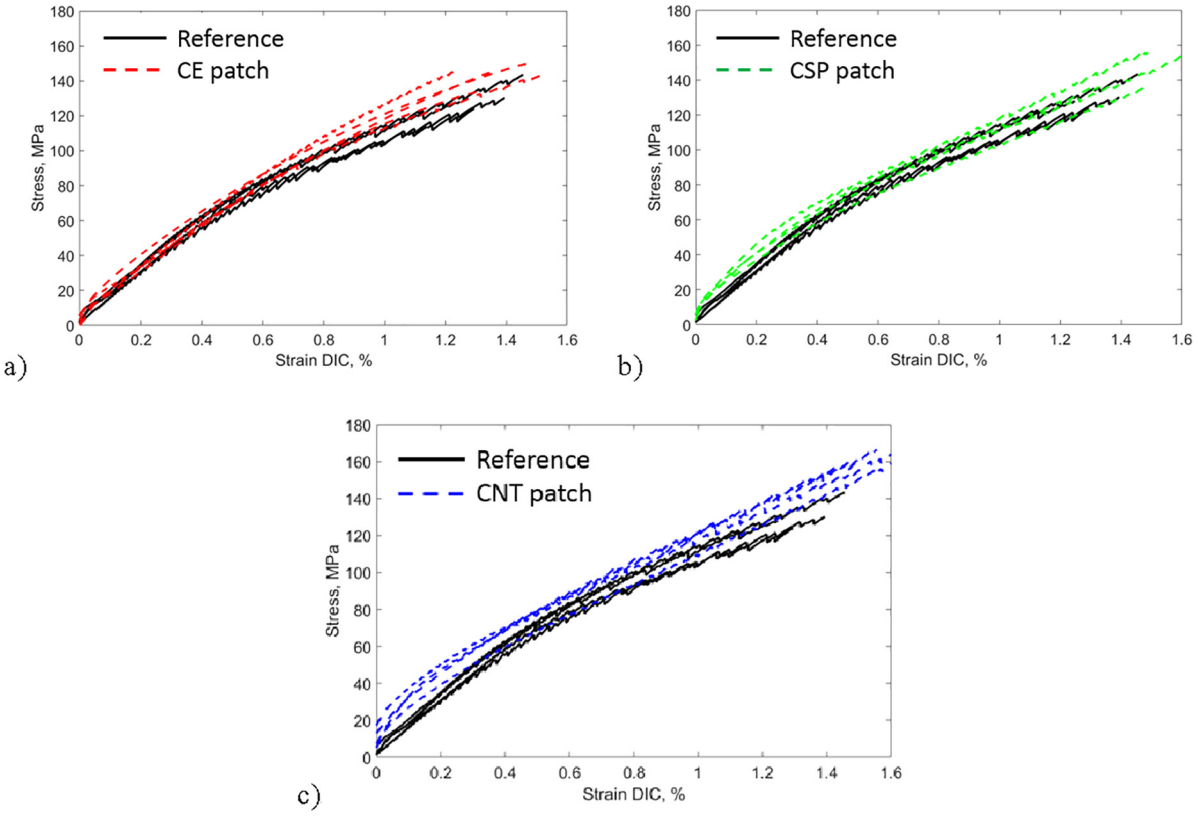

Fig. 3. Stress-strain diagrams of reference samples and patched samples: a) CE patch, b) CSP Rubber patch, c) CNT patch.

It is interesting to note, that the load bearing capacity of the fibre steered samples did not drop compared to non-steered samples despite the two factors that could negatively affect the load bearing capacity. First, the areal density of the preform around the hole, and hence the thicknesses, was 25% lower than in the reference sample (comparable to the thickness of one ply). The second factor is the additional bending stress in the axial yarns caused by the thickness variation. The incorporation of the CSP patched composite led to a further increase in the strength, reaching 14.5% compared to the steered non-patched samples and a remarkable 43% improvement compared to the non-patched and non-steered samples. On the other hand, the CNT patched samples did not reveal any pronounced difference to the non-patched steered samples.

The fibre steering appeared to have a significant effect on the composite damage accumulation mechanism. Local steering of the yarns led to much higher crack density away from the hole than in the hole vicinity. However, no difference in fracture zone size and type, between the patched and non-patched samples, can be immediately discerned. The presence of the patches in steered samples, on the other hand, did not cause any noticeable damage associated with the interface between the injected and the infused resins.

4. Discussion

Testing of braided composites revealed potential for improving composite performance through employing two concepts: (a) grading composite properties through local integration of resin with locally modified properties and (b) fibre steering through continuous variation

Table 1
Mechanical properties of patched and reference samples (highlighted cells indicate properties where the analysis of variation indicated significant difference compared to the reference batch).

Properties		No patch (reference)	CE patch	CSP patch	CNT patch
Apparent stiffness, GPa	Average	14.34	13.05	13.45	12.07
	Stdv	0.85	0.88	1.58	0.49
Strength, MPa	Average	131.32	143.75	148.50	163.80
	Stdv	8.44	5.92	13.66	3.04
Strain to failure, %	Average	1.35	1.38	1.51	1.58
	Stdv	0.09	0.12	0.15	0.06

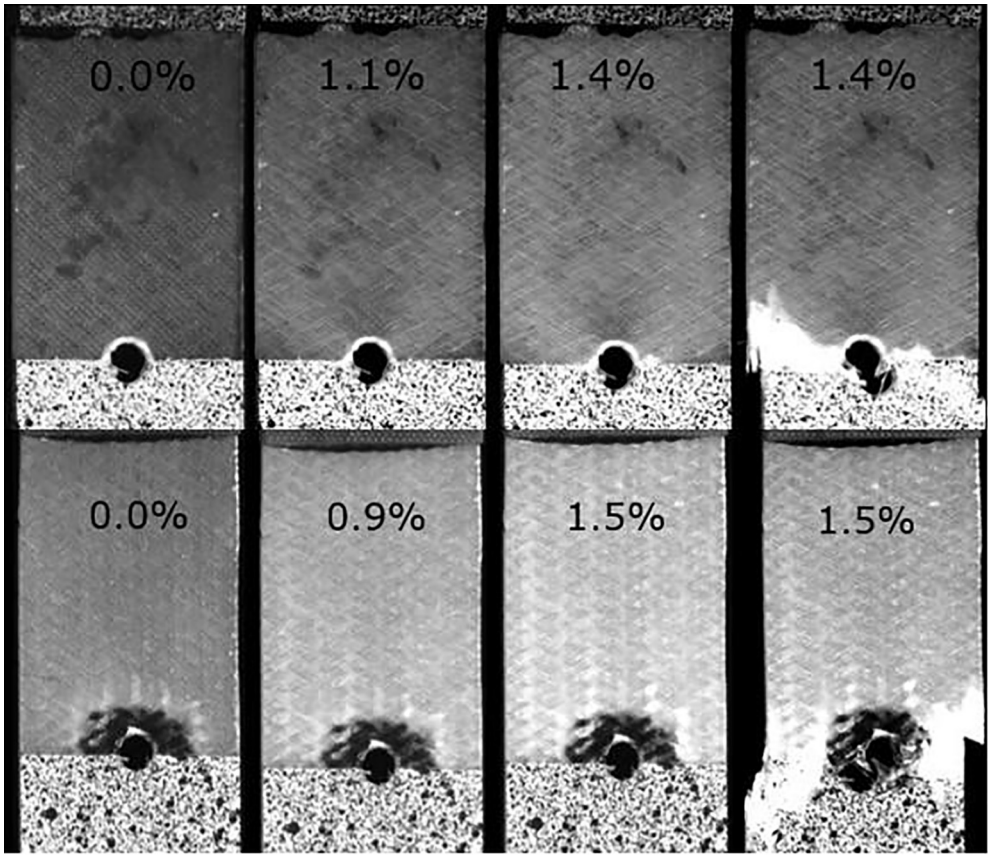

Fig. 4. Development of damage in reference (top) and CNT-patched (bottom) samples: unloaded (left), advanced damage stage (second from left), image taken a second before the failure (third from left), failure (right). Strain at which the damage is observed is shown on the images.

Table 2
The aspect ratio of the initially circular hole for CNT-patched and reference samples.

	No patch (reference)	CNT patch
At 1% strain, %	1.06–1.10	1.04–1.05
At failure	1.15–1.18	1.05–1.11

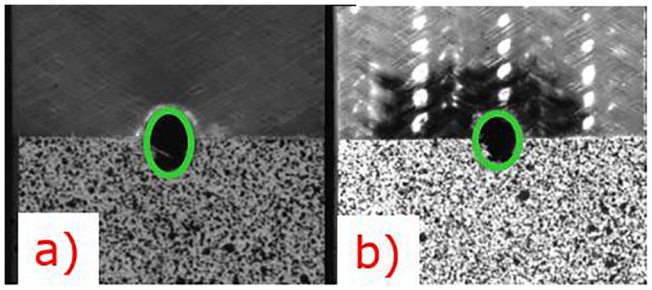

Fig. 5. The apparent difference between the deformation of the hole before failure in (a) the reference (b) and CNT-patched sample.

of braiding angle. The potential of these concepts was demonstrated both in isolation and in combination, leading to a pronounced improvement in strength of the open-hole samples. Different additives appeared to be beneficial for the two different braid configurations. In the nominal braid, without fibre steering, a significant difference was only observed for the material with the CNT enhanced patches. On the other hand, in the steered configurations the introduction of the toughened patch revealed a pronounced increase in the composite strength compared to steered non-patched samples.

A simple finite element analysis can be utilised to explain these effects. In the absence of precise data on strength and stiffness distribution within the patch, this model was aimed at obtaining a qualitative assessment of the deformation mechanisms, and not at detailed analysis of the studied materials, as for instance in yarn-scale models of conventional textile composites by Lomov et al. [22] and Ivanov et al. [23]. The model considered in this paper explored what impact grading/steering on stress peak values for a range of theoretically possible patch stiffnesses.

The complex sample geometry was presented as consisting of three areas with distinctly different properties: (a) an area with nominal properties of $0^{\circ}/\pm 60^{\circ}$ braid, (b) an area with properties of $0^{\circ}/\pm 45^{\circ}$, away from the grips in the steered samples, and (c) the patch zone modelled as a ring around the hole – Fig. 8. The stiffness in the patch zone can be adjusted based on assumed higher or lower stiffness of the matrix and on the braiding angle in the patch.

The yarn architecture in the braided composites is approximated with a laminate. Plies in this laminate correspond to axial yarns, braiding $+45^{\circ}$ yarns and braiding -45° yarns, while the ply fraction is set according to the relative weight fraction of braiding (80%) to axial (20%) yarns in the dry braid. The stiffness of each zone is calculated using Chamis's formulae [21], assuming the volume fraction of fibres in each of the plies is 42% for non-steered and 46% for the steered configurations. These values correspond to the overall fibre volume fraction in the composite. The stiffness in the patches is calculated based on two extreme assumptions about the matrix properties within patches: high stiffness (Young's modulus is three times higher than the one of host matrix) and low stiffness (Young's modulus is 10 times lower). The high stiffness estimate corresponds to a possible stiffening effect of CNTs, whereas the lower stiffness addresses the assumption that hypothetical defects are present, associated with porosity, thermal

Table 3
Mechanical properties of steered and patched steered samples (highlighted cells indicate properties where the analysis of variation indicated significant difference compared to the reference batch).

		No patch, no steering	No patch, steered	Steered and CSP patch	Steered and CNT patch
Apparent stiffness, GPa	Average	14.34	12.83	14.75	12.47
	Stdv	0.85	0.18	0.27	0.57
Strength, MPa	Average	131.32	164.63	188.64	154.74
	Stdv	8.44	1.85	8.93	2.90
Strain to failure, %	Average	1.35	1.50	1.60	1.46
	Stdv	0.09	0.06	0.13	0.06

cracking, or weak internal interfaces have a severe impact on stiffness. The actual stiffness of the patch is not known but optical strain measurements indicated that the material with incorporation of CNT patches does increase the stiffness, as revealed by the lower aspect ratio of the hole – Table 2, Fig. 5. Local thickness reduction in the steered region is not explicitly taken into account by the model.

The laminate plate theory (LPT) is used to calculate the stiffness in each of the zones. A 2D linear elastic plane stress FE model is then implemented in Abaqus to calculate the stress distribution at the macro level. The linear brick element (C3D8R) with reduced integration is used to mesh the part. The linear size of the elements in the proximity of the hole of 0.25 mm provides mesh independent results. The samples are loaded by a displacement applied in the x-direction, shear traction free surfaces are assumed both on the symmetry planes and at the loaded surface. To make the results comparable between the steered and non-steered configuration, the displacement is set to provide the same total strain (*i.e.* the strain in an equivalent sample without the hole). Once the macro strain is calculated LPT is used to derive the local stresses at the ply level.

Fibre rupture and sample disintegration can be assumed to occur when the x-component of direct stress in the axial plies reaches a critical value. Peak longitudinal stress in fibres is indicative to the probability of fibre rupture. Such criterion, though simplistic, is adequate for revealing one of the most important consequences of grading. Hence, the decrease of the peak value compared to the reference configurations points at possible improvements in the strength of the open hole samples. The results are summarised in Table 4. Overall, this model explains most of the experimentally observed results from a qualitative standpoint. In both the non-steered and steered configurations, the increase of the patch stiffness leads to a reduction of peak stresses in the axial plies; lowering stiffness had the opposite effect. These effects occur because the strain at the macro level is not significantly influenced by the local modification of stiffness, whereas at the ply scale a larger fraction of the load is taken by off-axis yarns where the matrix is stiffer. In general, steering leads to the same level of axial peak stress in the non-patched materials. The same level of predicted stresses in steered and non-steered samples is consistent with the observation that a similar load at failure was observed for steered and non-steered samples and the difference in the stress-strain curves arises when the load is normalised with respect to the sample thickness at the failure location.

Table 4
Normalised peak stresses in the axial yarns for different material configurations with respect to the reference (not steered, not patched).

	Low stiffness patch	No patch	High stiffness patch
Non-steered braid	1.17	1.0	0.83
Steered braid	1.16	0.98	0.83
Steered braid with damage in ± 60° yarns	1.08	0.91	0.77

The apparent increase in strength of the open hole samples with the CNT patches supports the assumption that the nano-reinforcement led to a local stiffening, whereas the integration of the CSP or CE patches did not lead to any noticeable impact on the stiffness distribution. The

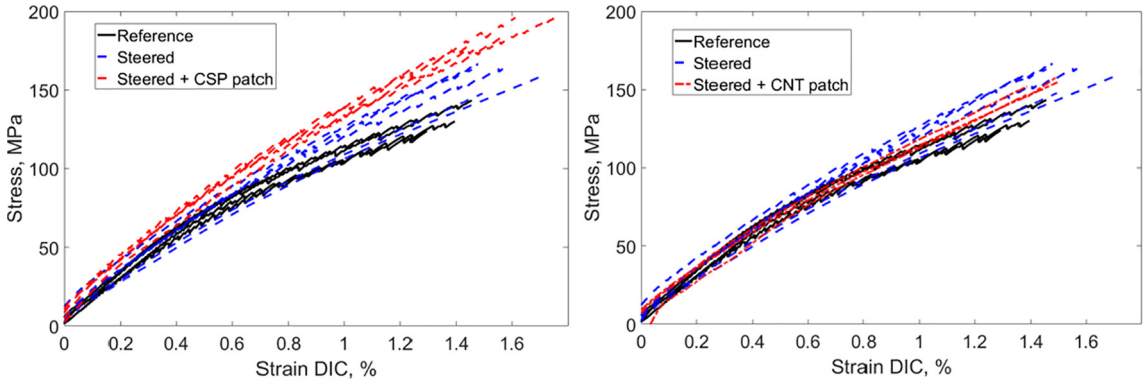

Fig. 6. Stress-strain diagrams reference samples, steered sample, and steered and patched with rubber particles samples.

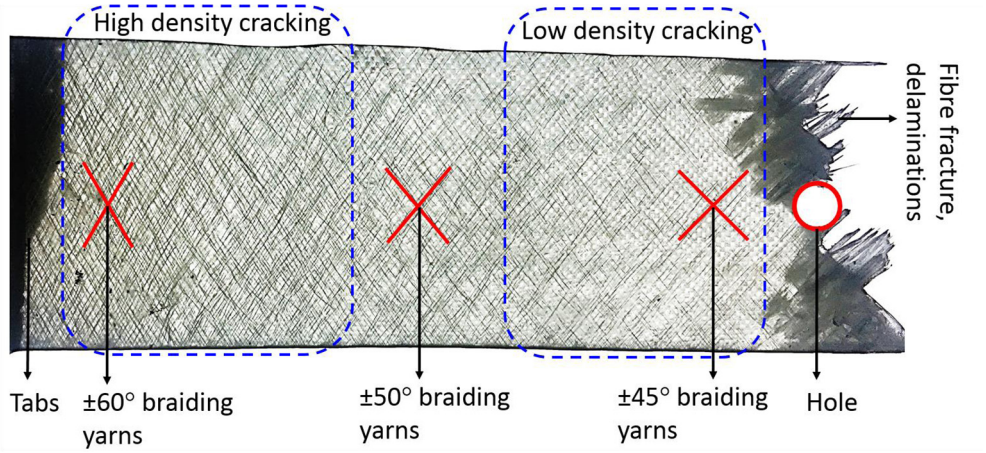

Fig. 7. Fractured steered braided composite (no patch) in transmitted light showing variation in transverse matrix cracking over the sample length and failure zone.

model does not capture the increase in load to failure when the CSP patch is introduced. To explain this phenomenon, our attention needs to be directed away from the patch zone. As shown in Fig. 7, the steered samples exhibited a very peculiar damage pattern – an intensive crack accumulation happens away from the stress concentration. In the glass-epoxy samples, the cracking leads to a noticeable decrease in stiffness. The damaged area undergoes higher deformation, which means that for a given applied strain (as in the displacement-controlled tests described above) the macro-strain at the hole is lower than it could have been without cracking. Lower macro-strains lead to lower peak stresses in the axial yarns. To assess the validity of such an assumption, the 0°/ ± 60° zone can be assigned with the properties of the damaged material. The precise degradation factor is unknown but the model of Zinoviev [24] provides a sensible and simple estimate. It suggests that the local stress across the yarns in the transverse direction does not increase throughout the damage accumulation process. Hence, for a given estimate of the transverse strength of axial yarns (54 MPa) and strain in braiding yarns at failure (1.07%), one can find a reasonable value of braiding yarn stiffness at sample disintegration (3.97 GPa compared to the initial stiffness of 9.15 GPa). LPT is then used to calculate the macro stiffness of the degraded area: Young's modulus 11.6 GPa compared to the initial modulus of 13.7 GPa. This simple model does show that damage away from the stress concentrator leads to lower stresses in fibres at the direct vicinity of stress concentrator – Table 4. The peak stresses in the steered configuration are seen to decrease by 9% with damage accumulation in the 0°/ ± 60° zone. A further reduction up to 23% is observed on addition of a stiffer patch around the hole in the steered configuration.

Hence, this exercise leads us to a non-trivial conclusion: steering does have the potential to improve the strength through damage accumulation. The critical factor for this improvement is that the stiffness degradation should occur away from the stress concentrator but on a path between the location of peak stress and load application. This mechanism is realised independently from the strength improvement due to matrix grading. It does not entirely explain why an improvement in strength was seen in the case of the CSP patch but not for the CNT patch in the steered configuration. The possible explanation is that the rubber patch toughen the material, preventing damage accumulation even at high strain levels, whereas the integration of stiff CNT clusters may promote damage. Cracking in the vicinity of the hole may impede the actuation of strain-relief mechanisms.

5. Conclusions

The study showed several ways to improve the strength of composites with stress concentration that can be applied in isolation and in combination. Increased strength was realised through ***matrix grading***: local integration of stiff or tough matrices and by ***fibre steering***: varying braid angle and preform density along the length of the sample. The effect of fibre steering was particularly obvious in two aspects: (1) decreasing sample thickness and areal density at the critical location without compromising the load at failure, hence more reinforcing plies can be added in the critical location without affecting thickness or weight penalty, (2) redirecting damage accumulation away from the stress concentrator and hence, releasing the peak stresses in overloaded areas. The cumulative effect of these mechanisms allowed an

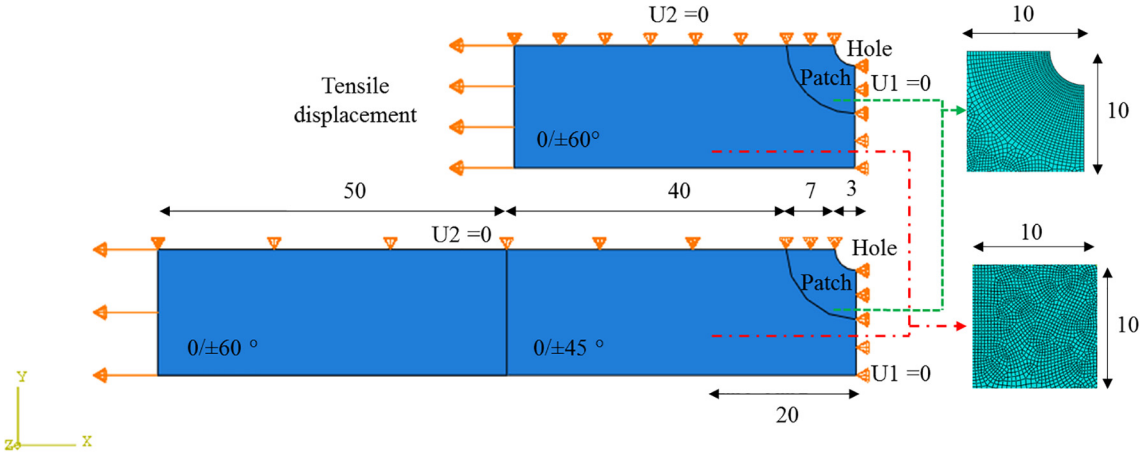

Fig. 8. Sketch of finite element model for simplified non-steered and steered configurations (all dimensions in mm).

improvement in strength of more than 40%.

Matrix grading was implemented by integration of resins *via* multiple injections through the thickness at selected locations. This method proved to be efficient to incorporate a large fraction of additives, bypassing the common limitations of liquid moulding associated with elevated viscosity. Short flow lengths provide a possibility to introduce large loading of additives that significantly affect the local stiffness. The boundaries of the particle concentration could easily be increased in future. The filtration mechanism around the injection zone provided natural mechanisms of grading and a smooth transition between dissimilar matrices. Patterned combinations of resins systems within one composite structure has clear potential to improve overall composite component performance.

The results were obtained for a relatively compliant composite in which the matrix makes a noticeable contribution to the composite stiffness. Hence, it is not possible to directly extrapolate the observed improvement to other material systems. For instance, in carbon composites the contrast between matrix and fibre stiffness is much larger, and the degradation caused by matrix cracking has little influence on the stiffness in fibre dominated directions. However, by increasing additive content, and by integrating advanced nano- and micro-reinforcements, similar effects may be realised even in high-performance materials.

A simplified model has been used to explain the mechanisms that result in the improvement shown in steered configurations. The model suggests a design window for further optimising the selection of matrices for the patch. Further work is needed to understand the exact mechanism of redistributing the load and failure around matrix graded zones. However, it is clear that matrix grading provides a potential solution to achieve tougher and more resilient composites.

Acknowledgments

The work of Dr. Ivanov was supported by EPSRC grant EP/M009149/1 ‘New generation of manufacturing technologies: liquid print of composite matrices’, the contribution of Professor Potluri and Dr. Roy was facilitated by EPSRC Henry Royce Pump Priming: ‘Gradient reinforcements and matrices for resilient feature insensitive composites’ and the work of Arjun Radhakrishnan was supported by the Engineering and Physical Sciences Research Council through the EPSRC Centre for Doctoral Training in Advanced Composites for Innovation and Science (grant number EP/L016028/1). Authors express gratitude to Huntsman Advanced Materials for providing some of the resin systems used in the study and advice.

References

[1] Udupa G, Rao SS, Gangadharan KV. Functionally graded composite materials: an overview. Procedia Mater Sci 2014;5:1291–9.
[2] Carbas RJC, da Silva LFM, Critchlow GW. Adhesively bonded functionally graded joints by induction heating. Int J Adhes Adhes 2014;48:110–8.
[3] Jha DK, Kant T, Singh RK. A critical review of recent research on functionally graded plates. Compos Struct 2013;96:833–49.
[4] Erb RM, Libanori R, Rothfuchs N, Studart AR. Composites reinforced in three dimensions by using low magnetic fields. Science 2012;335:6065.
[5] Fratzl P. Cellulose and collagen: from fibres to tissues. Curr Opin Colloid Interface Sci 2003;8(1):32–9.
[6] Huang Z, Wang Q, Ramakrishna S. Tensile behaviour of functionally graded braided carbon fibre. Epoxy Composite Mater 2002;10(4):307–14.
[7] Kieback B, Neubrand A, Riedel H. Processing techniques for functionally graded materials. Mater Sci Eng A 2003;362(1–2):81–106.
[8] Fink BK, Gillespie J, Gillio E, Bernetich K. One-step resin transfer molding of multifunctional composites consisting of multiple resins. Google Patents; 2000.
[9] Gillio EF, McKnight GP, Gillespie JW, Advani SG, Bernetich KR, Fink BK. Processing and properties of co-injected resin transfer molded vinyl ester and phenolic composites. Polym Compos 1999;20(6):780–8.
[10] Harkare A, Gillespie Jr JW. In situ barrier layer formation for coinjection resin transfer molding. J Thermoplast Compos Mater 2004;17(5):387–409.
[11] Krollmann J, Alvarado CS, Carqueville P, Snajdr R, Zaremba S, Drechsler K. Hybrid-matrix processing: how to co-inject multiple resin systems into one composite part ?. In: ECCM17-17th European Conference on Composite Materials; 2016, vol. c, no. June. p. 26–30.
[12] Ivanov DS, White JAP, Hendry W, Mahadik Y, Minett V, Patel H, et al. Stabilizing textile preforms by means of liquid resin print: a feasibility study. Adv Manuf Polym Compos Sci Feb. 2015;1(1):26–35.
[13] Ivanov DS, Le Cahain YM, Arafati S, Dattin A, Ivanov SG, Aniskevich A. Novel method for functionalising and patterning textile composites: liquid resin print. Compos Part A Appl Sci Manuf 2016;84:175–85.
[14] Wisnom MR, Hallet SM. The role of delamination in strength, failure mechanism and hole size effect in open hole tensile tests on quasi-isotropic laminates. Compos Part A Appl Sci Manuf 2009;40(4):335–42.
[15] Stanier D, Gent I, Roy SS, Hamerton I, Potluri P, Ivanov D. Mechanical behaviour of patterned multi-matrix composites with gradient properties. In: ECCM 2016 – Proceeding of the 17th European Conference on Composite Materials, European Conference on Composite Materials, ECCM, 2016.
[16] Fang T, Shimp DA. Polycyanate esters: science and applications. Prog Polym Sci 1995;20(1):61–118.
[17] Hamerton I. Introduction to cyanate ester resins. Chemistry and technology of cyanate ester resins. Springer; 1994. p. 1–6.
[18] Herceg T. Nano and hierarchical composites with high CNT loading fractions. Imperial College London; 2013.
[19] Zainol Abidin MS. Development of hierarchical composites for structural applications. Imperial College London; 2015.
[20] Ivanov DS, Baudry F, Van Den Broucke B, Lomov SV, Xie H, Verpoest I. Failure analysis of triaxial braided composite. Compos Sci Technol 2009;69(9):1372–80.
[21] Chamis CC. Simplified composite micromechanics equations for hygral, thermal and mechanical properties; 1984.
[22] Lomov SV, Bernal E, Ivanov DS, Kondratiev SV, Verpoest I. Homogenisation of a sheared unit cell of textile composites: FEA and approximate inclusion model. Eur Finite Elem Rew 2005;14(6–7):709–29.
[23] Ivanov DS, Lomov SV, Baudry F, Xie H, Van Den Broucke B, Verpoest I. Failure analysis of triaxial braided composite. Compos Sci Technol 2009;69(9):1372–80.
[24] Zinoviev PA, Grigoriev SV, Lebedeva OV, Tairova LP. The strength of multilayered composites under a plane-stress state. Compos Sci Technol 1998;58(7):1209–23.